nature medicine

Reconstruction of the mouse extrahepatic biliary tree using primary human extrahepatic cholangiocyte organoids

Fotios Sampaziotis[1–3], Alexander W Justin[4], Olivia C Tysoe[1,2], Stephen Sawiak[5,26], Edmund M Godfrey[6,26], Sara S Upponi[6,26], Richard L Gieseck III[7], Miguel Cardoso de Brito[1,2], Natalie Lie Berntsen[8], María J Gómez-Vázquez[9], Daniel Ortmann[1,2], Loukia Yiangou[1,10,11], Alexander Ross[1,12,13], Johannes Bargehr[1,10,11,14], Alessandro Bertero[1,2], Mariëlle C F Zonneveld[1], Marianne T Pedersen[15], Matthias Pawlowski[1], Laura Valestrand[8], Pedro Madrigal[1,16], Nikitas Georgakopoulos[2], Negar Pirmadjid[2], Gregor M Skeldon[17,18], John Casey[19], Wenmiao Shu[17,18], Paulina M Materek[20], Kirsten E Snijders[1], Stephanie E Brown[1,2], Casey A Rimland[1,2,7,21], Ingrid Simonic[22], Susan E Davies[23], Kim B Jensen[13], Matthias Zilbauer[1,11], William T H Gelson[3], Graeme J Alexander[10,11], Sanjay Sinha[1,12], Nicholas R F Hannan[24,25], Thomas A Wynn[7], Tom H Karlsen[8], Espen Melum[8], Athina E Markaki[4], Kourosh Saeb-Parsy[2,27] & Ludovic Vallier[1,2,16,27]

The treatment of common bile duct (CBD) disorders, such as biliary atresia or ischemic strictures, is restricted by the lack of biliary tissue from healthy donors suitable for surgical reconstruction. Here we report a new method for the isolation and propagation of human cholangiocytes from the extrahepatic biliary tree in the form of extrahepatic cholangiocyte organoids (ECOs) for regenerative medicine applications. The resulting ECOs closely resemble primary cholangiocytes in terms of their transcriptomic profile and functional properties. We explore the regenerative potential of these organoids *in vivo* and demonstrate that ECOs self-organize into bile duct–like tubes expressing biliary markers following transplantation under the kidney capsule of immunocompromised mice. In addition, when seeded on biodegradable scaffolds, ECOs form tissue-like structures retaining biliary characteristics. The resulting bioengineered tissue can reconstruct the gallbladder wall and repair the biliary epithelium following transplantation into a mouse model of injury. Furthermore, bioengineered artificial ducts can replace the native CBD, with no evidence of cholestasis or occlusion of the lumen. In conclusion, ECOs can successfully reconstruct the biliary tree, providing proof of principle for organ regeneration using human primary cholangiocytes expanded *in vitro*.

Disorders of the extrahepatic bile duct carry considerable morbidity and mortality. Indeed, 70% of pediatric liver transplantations are performed to treat biliary atresia[1], while primary sclerosing cholangitis (PSC) alone accounts for 5% of liver transplantations in the United States[2] and biliary complications are the leading cause of graft failure following deceased donor liver transplantation[3,4]. Treatment options remain limited[5,6] owing to the lack of healthy donor tissue that can be used to reconstruct and replace diseased bile ducts. *In vitro* expansion of native cholangiocytes could address this limitation and provide cells suitable for tissue engineering applications such as biliary reconstruction. However, the culture of primary biliary epithelium remains problematic[7]. Here we report a new method, compatible with regenerative medicine applications, for the isolation and propagation of primary human cholangiocytes from the extrahepatic biliary tree. The resulting ECOs express key biliary markers, such as cytokeratin 7 (KRT7 or CK7), cytokeratin 19 (KRT19 or CK19), γ-glutamyl transferase (GGT) and cystic fibrosis transmembrane conductance regulator (CFTR), and maintain their functional properties *in vitro*, including alkaline phosphatase (ALP) and GGT activity and responses to secretin and somatostatin. The potential of ECOs in tissue engineering and clinical applications is further illustrated by their capacity to populate biodegradable scaffolds, organize into a functional biliary epithelium and rescue a mouse model of extrahepatic biliary injury (EHBI).

RESULTS

Human extrahepatic cholangiocytes can be propagated as organoids

We first focused on identifying the optimal conditions under which to isolate primary cholangiocytes from the biliary epithelium, which forms a monolayer covering the luminal surface of the biliary tree[8]. We tested several approaches for recovering these cells (**Supplementary Fig. 1a–c**); mechanical dissociation by brushing or scraping the bile duct luminal surface was associated with improved survival of the cholangiocytes as compared to enzymatic digestion

A full list of affiliations appears at the end of the paper.

Received 11 July 2016; accepted 24 May 2017; published online 3 July 2017; doi:10.1038/nm.4360

of the bile duct (**Fig. 1a** and **Supplementary Fig. 1a**). Furthermore, the majority of the cells resulting from mechanical dissociation coexpressed the biliary markers CK7 and CK19 (94.6% ± 2.4%, s.d.; $n = 3$ independent dissociation experiments), and no contamination from mesenchymal cell types was detected (**Supplementary Fig. 1d**). Consequently, mechanical dissociation constitutes the optimal method for isolating extrahepatic cholangiocytes.

To discern appropriate conditions for the maintenance and propagation of these cells, we optimized our recently established system for 3D culture of intrahepatic cholangiocytes derived from human induced pluripotent stem cells[9,10]. Screening of multiple growth factors known to support the expansion of both cholangiocytes and epithelial organoids[11,12] (**Supplementary Fig. 1b**,**c**) identified the combination of epidermal growth factor (EGF), R-spondin and Dickkopf-related protein 1 (DKK-1) as sufficient to promote the growth of primary cholangiocytes into organoids (**Supplementary Fig. 1c**). Because of the paradoxical requirement for both a Wnt potentiator (R-spondin) and a Wnt inhibitor (DKK-1), we characterized the activity of both the canonical and noncanonical (planar cell polarity, PCP) Wnt pathways in ECOs. Our results demonstrate higher β-catenin phosphorylation in ECOs than in cells treated with R-spondin but not DKK-1 (**Supplementary Fig. 1e**,**f**), signifying lower canonical Wnt pathway activity in these cells. Furthermore, ECOs exhibited higher Rho kinase activity than cells treated with R-spondin but not DKK-1 (**Supplementary Fig. 1g**), which could be consistent with enhanced signaling through the noncanonical PCP pathway in ECOs. Thus, it is possible that noncanonical Wnt signaling controls ECO expansion, marking a notable difference with previous organoid culture conditions[12].

Under these conditions, we derived eight different ECO lines (**Fig. 1a–d**, **Supplementary Figs. 2a–f** and **3a–e**, and **Supplementary Table 1**) from a variety of deceased donors aged 33–77 years. Notably, we obtained similar results by using cholangiocytes isolated from the gallbladder or by isolating CBD cholangiocytes using an endoscopic retrograde cholangiopancreatography (ERCP) brush instead of scraping the luminal surface (**Supplementary Fig. 2a**,**b**). Consequently, ECOs can be derived from different areas of the extrahepatic biliary tree and collected using perioperative (dissection and scraping) or minimally invasive (ERCP brushing) approaches.

ECOs maintain expression of key biliary markers and functional properties in culture

The resulting cells were expanded *in vitro* for prolonged periods of time (**Supplementary Fig. 4a**), during which they maintained their genetic stability (**Supplementary Fig. 4b**,**c**). Electron microscopy revealed the presence of ultrastructural features characteristic of cholangiocytes, including cilia, microvilli and tight junctions[13] (**Supplementary Fig. 3c**), while qRT–PCR and immunofluorescence (IF) analyses established the expression of key biliary markers, including KRT7, KRT19, hepatocyte nuclear factor-1β (HNF-1β), GGT, secretin receptor (SCTR), sodium-dependent bile acid transporter (SLC10A2; also known as ASBT), CFTR and SRY-box 9 (SOX9)[9] (**Fig. 1b**,**c** and **Supplementary Figs. 2c**,**d** and **3d**,**e**). Of note, expression was not detected for stem cell markers, such as OCT4 (POU5F1), NANOG, prominin 1 (PROM1) and leucine-rich-repeat-containing G-protein-coupled receptors (LGR family: LGR4, LGR5 and LGR6); for markers of non-biliary lineages, including albumin (ALB), α_1-antitrypsin (A1AT; also known as SERPINA1), keratin 18 (KRT18), pancreatic and duodenal homeobox-1 (PDX1), insulin (INS) and glucagon (GCG); or for epithelial–mesenchymal transition (EMT) markers, such as vimentin (VIM), snail family transcriptional repressor 1 (SNAI1) and S100 calcium-binding protein A4 (S100A4) (**Supplementary Fig. 5a–c**). On the other hand, 98.1% ± 0.9% (s.d.) of the cells ($n = 3$ cell lines) coexpressed CK7 and CK19 following 20 passages in culture (**Supplementary Fig. 1d**), thereby confirming the presence of a nearly homogeneous population of cholangiocytes.

Transcriptomic analyses (**Fig. 1d**, **Supplementary Fig. 6** and **Supplementary Table 2**) revealed that ECOs maintained a stable gene expression profile over multiple passages (Pearson correlation coefficient for passage 1 versus passage 20 ECOs, $r = 0.99$; **Supplementary Fig. 6a**,**b**), expressed key biliary markers (**Supplementary Fig. 6c**) and clustered closely to freshly isolated cholangiocytes (**Supplementary Fig. 6d**) (Pearson correlation coefficient for primary cholangiocytes versus passage 20 ECOs, $r = 0.92$; **Supplementary Fig. 6b**). Gene ontology (GO) analyses confirmed enrichment of pathways that are typically activated in the biliary epithelium (**Supplementary Fig. 6e**). When considered collectively, these results demonstrate that primary cholangiocytes derived from the extrahepatic biliary tree can be expanded *in vitro* without losing their original characteristics.

We then further characterized ECOs by focusing on their function following long-term culture (20 passages). Biliary epithelium regulates the homeostasis of bile through transport of ions, water and bile acids[8,14]. The secretory capacity of ECOs was interrogated using rhodamine 123, a fluorescent substrate for the cholangiocyte surface glycoprotein multidrug resistance protein-1 (MDR1)[15,16] (**Fig. 2a–c**). Rhodamine 123 accumulated in the ECO lumen only in the absence of the MDR1 antagonist verapamil, thereby confirming active secretion through MDR1 (**Fig. 2a–c**). Luminal extrusion of bile acids[17] was also demonstrated by showing that the fluorescent bile acid cholyl-lysyl-fluorescein (CLF) was actively exported from ECOs (**Fig. 2d–f**). Furthermore, ALP and GGT activities in ECOs were comparable to those in freshly plated primary cholangiocytes (**Fig. 2g**,**h** and **Supplementary Fig. 2e**,**f**). The response of ECOs to secretin and somatostatin was also assessed. Secretin promotes water secretion, resulting in distension of the bile duct lumen, whereas somatostatin negates the effects of secretin[18–20]. Accordingly, organoids exposed to secretin increased their diameter as compared to untreated controls, whereas somatostatin inhibited the effect of secretin (**Fig. 2i**,**j**). Our data therefore demonstrate that ECOs maintain their functional properties after long-term culture.

ECOs self-organize into bile duct–like tubes after transplantation

These results prompted us to investigate the potential of ECOs for *in vivo* use, especially in regenerative medicine applications. We first characterized the potential of ECOs to engraft and survive *in vivo* by transplanting cells under the kidney capsule of NOD.Cg-*Prkdc*^{scid}*Il2rg*^{tm1Wjl} (NSG) mice (**Supplementary Fig. 7a**) and maintaining the mice for 12 weeks[21]. ECOs were successfully engrafted, forming tubular structures expressing biliary markers such as CK19 (**Supplementary Fig. 7b–d**).

Notably, no tumor formation or expression of markers for differentiation into other lineages was detected (**Supplementary Fig. 7d**). Thus, ECOs appear to maintain their basic characteristics even after prolonged engraftment *in vivo* under the kidney capsule.

ECO-populated scaffolds reconstruct the gallbladder wall

To assess the potential of ECOs for tissue engineering, we first interrogated their capacity to populate biodegradable polyglycolic acid (PGA) scaffolds, which are commonly used to provide the structural and mechanical support required for tissue reconstruction[22].

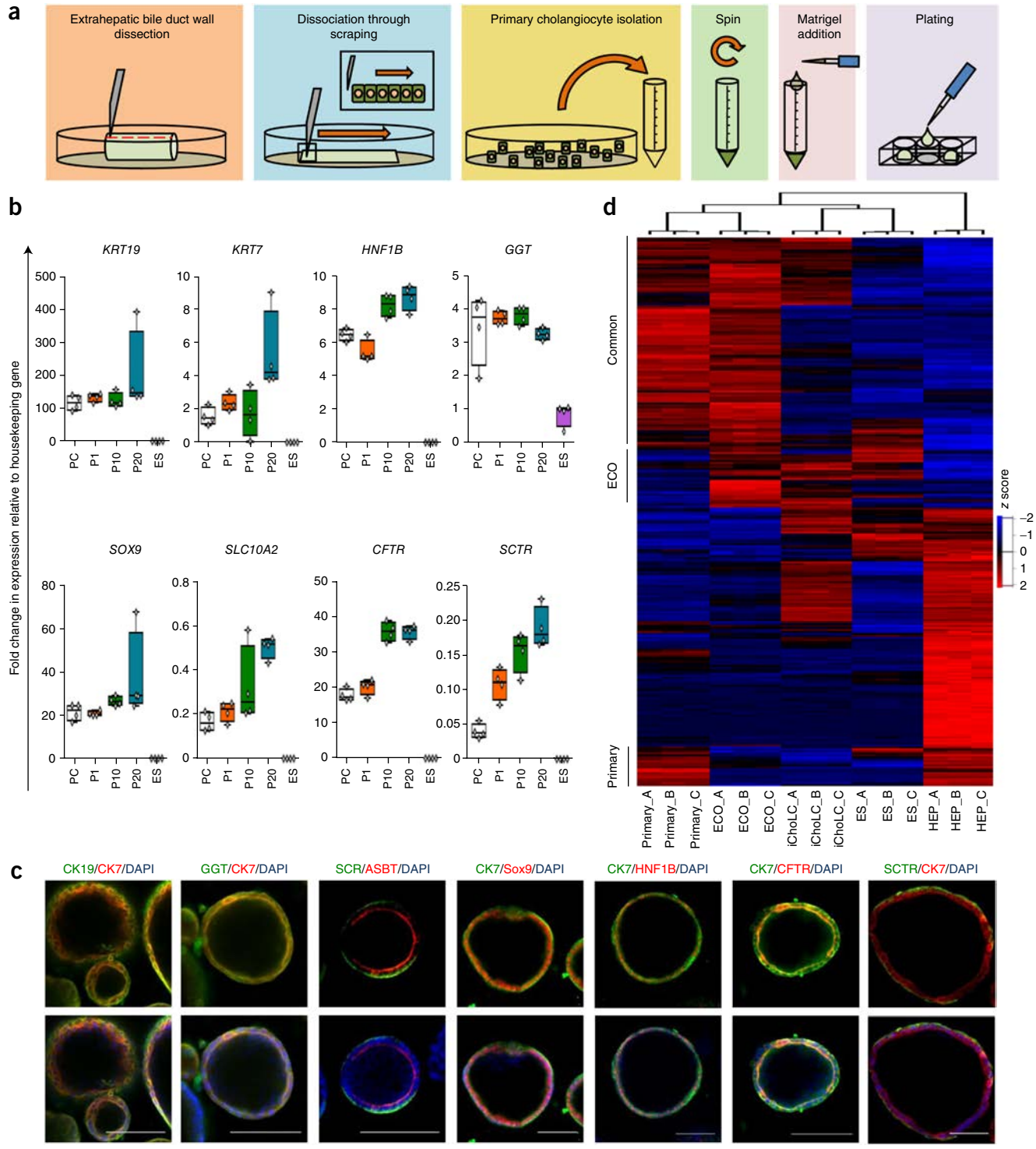

Figure 1 Derivation and characterization of ECOs. (**a**) Schematic representation of the method used for the derivation of ECOs. (**b**) qRT–PCR confirming the expression of biliary markers in ECOs after passage 1 (P1), passage 10 (P10) and passage 20 (P20) as compared to freshly isolated primary cholangiocytes (PC) and embryonic stem cells (ES) used as a negative control; $n = 4$ ECO lines. Center line, median; box, interquartile range (IQR); whiskers, range (minimum to maximum). Values are relative to those for the housekeeping gene *HMBS*, encoding hydroxymethylbilane synthase. (**c**) IF analyses confirming the expression of biliary markers by ECOs. Scale bars, 100 µm. Single-channel and higher-magnification images are provided in **Supplementary Figure 3**. (**d**) Euclidean hierarchical clustering analysis comparing the transcriptomes of primary cholangiocytes (Primary), passage 20 ECOs (ECO), human iPSC-derived intrahepatic cholangiocyte-like cells (iCholC), embryonic stem cells (ES) and hepatocytes (HEP). For each probe, standard scores (*z* scores) indicate differential expression, measured as the number of s.d. from the average expression level across all the samples. Clusters of genes expressed in ECOs, primary cholangiocytes or both cell types (common) are indicated. GO analyses for each cluster are provided in **Supplementary Figure 7e**. The data correspond to three samples for each cell type (A–C).

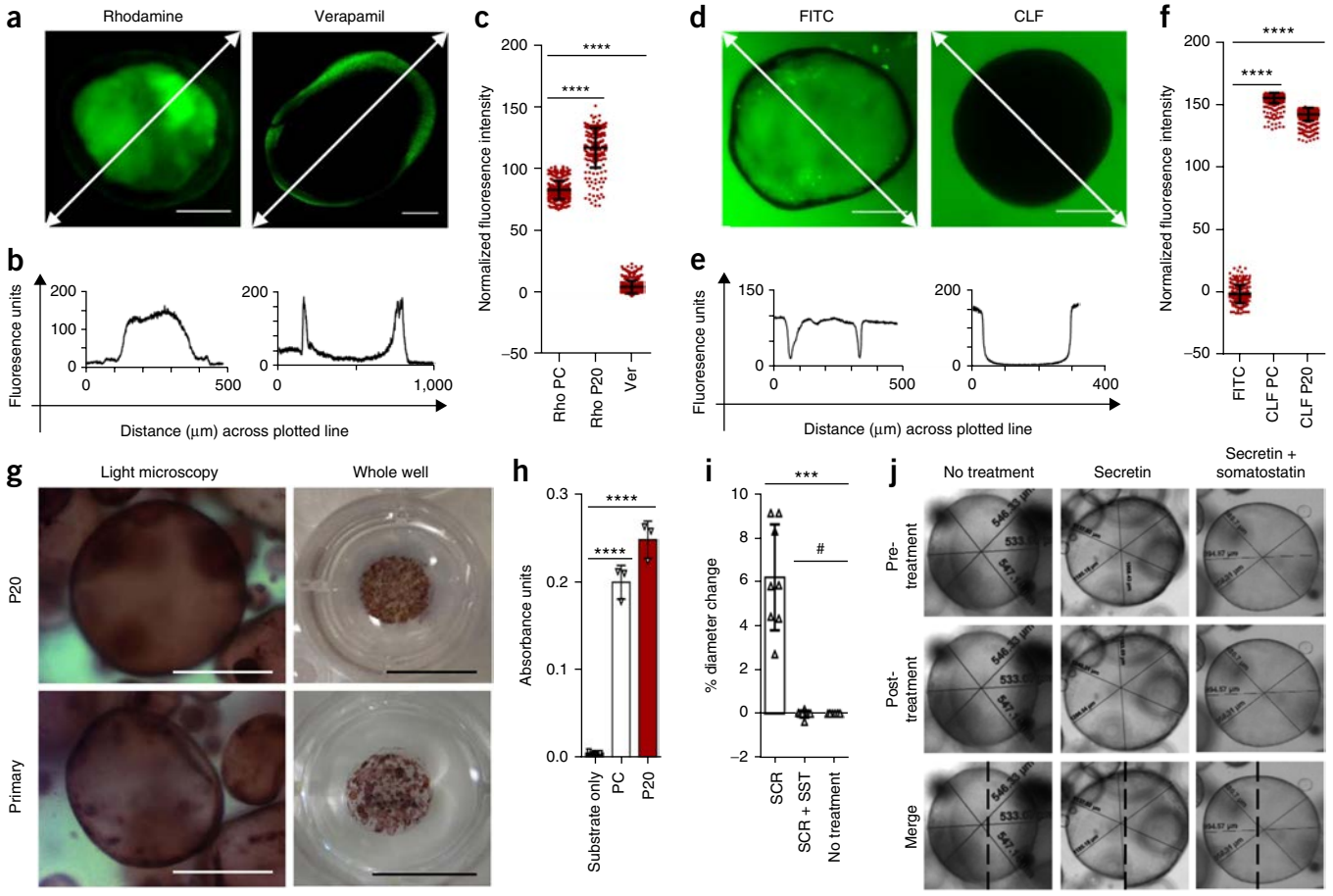

Figure 2 Functional characterization of ECOs. (**a**) Fluorescence images demonstrating secretion of fluorescent rhodamine 123, the substrate of MDR1, into the lumen of ECOs; secretion is inhibited by the MDR1 inhibitor verapamil. Scale bars, 100 μm. (**b**) Graphs depicting the fluorescence intensity along the white lines in the images in **a**. (**c**) Mean intraluminal fluorescence intensity normalized to background levels for freshly plated primary cholangiocytes (Rho PC), passage 20 ECOs (Rho P20) and passage 20 ECOs treated with verapamil (Ver). Error bars, s.d.; $n = 1{,}565$ measurements in total. $^{****}P < 0.001$, Kruskal–Wallis test with Dunn's correction for multiple comparisons. (**d**) Luminal extrusion of the fluorescent bile acid CLF as compared to controls loaded with FITC, confirming bile acid transfer. Scale bars, 100 μm. (**e**) Graphs depicting the fluorescence intensity along the white lines in the images in **d**. (**f**) Mean difference between intra- and extraluminal fluorescence intensity for control ECOs loaded with FITC (FITC), primary cholangiocytes loaded with CLF (CLF PC) and passage 20 ECOs loaded with CLF (CLF P20); $n = 1{,}947$ total measurements. Error bars, s.d.; $^{****}P < 0.001$, Kruskal–Wallis test with Dunn's correction for multiple comparisons. (**g**) Staining of ECOs and primary cholangiocytes for ALP activity. Scale bars, 500 μm (left) and 1 cm (right). (**h**) Mean GGT activity in passage 20 ECOs versus primary cholangiocytes. Error bars, s.d.; $n = 3$ cell lines; $^{****}P < 0.001$, one-way ANOVA with Dunnett's correction for multiple comparisons. (**i**,**j**) Mean diameter measurements (**i**) and live images (**j**) of ECOs treated with secretin or with secretin and somatostatin, demonstrating an increase in diameter following treatment with secretin. Error bars, s.d.; $n = 8$ organoids measured per condition; $^{***}P < 0.001$, $^{\#}P > 0.05$, Kruskal–Wallis test with Dunn's correction for multiple comparisons. Diameter measurements in micrometers are indicated on each image. Merged images show the diameter of the same organoid before (left) and after (right) the treatment indicated in the column. Before and after images are separated by a black dashed line. In **a**–**j**, data are representative of three different experiments.

Indeed, PGA is one of the most widely used synthetic polymers because it does not induce inflammatory responses in surrounding tissue, is biodegradable, and is more flexible and easier to process than natural polymers such as collagen[23]. To facilitate tracking of cells, ECOs expressing GFP were generated through viral transduction (**Supplementary Fig. 8**). The resulting GFP$^+$ ECOs were seeded on PGA scaffolds where they attached to the PGA fibers within 24–48 h and continued to grow for 4 weeks until they reached confluency (**Fig. 3a**–**d**). Of note, primary cholangiocytes grown under 2D conditions demonstrated limited expansion potential and failed to reach confluency when seeded on the scaffolds (**Supplementary Fig. 9**), suggesting that the proliferative capacity of ECOs is crucial for successful scaffold colonization. The populated PGA scaffolds (**Fig. 3b**,**c**) could easily be handled with forceps and divided into smaller pieces with a surgical blade. Furthermore, the cells populating the scaffolds retained expression of biliary markers such as CK7 and CK19 (**Fig. 3e**,**f**), demonstrated no evidence of EMT (**Fig. 3e**,**g**) and maintained their functional properties, including ALP and GGT activity (**Fig. 3h**,**i**). Therefore, ECOs can populate PGA scaffolds while maintaining their functionality and marker expression, thereby providing a bioengineered tissue resembling the biliary epithelium.

We then determined the capacity of ECOs to repair the biliary epithelium. To do so, we developed a mouse model of EHBI. More specifically, to simulate wall defects in the biliary tree requiring biliary reconstruction[24], the biliary trees of healthy NSG mice were compromised by longitudinal incision of the gallbladder wall (**Fig. 4a**). The surgical defect in the gallbladder wall was subsequently repaired by transplanting PGA scaffolds populated with

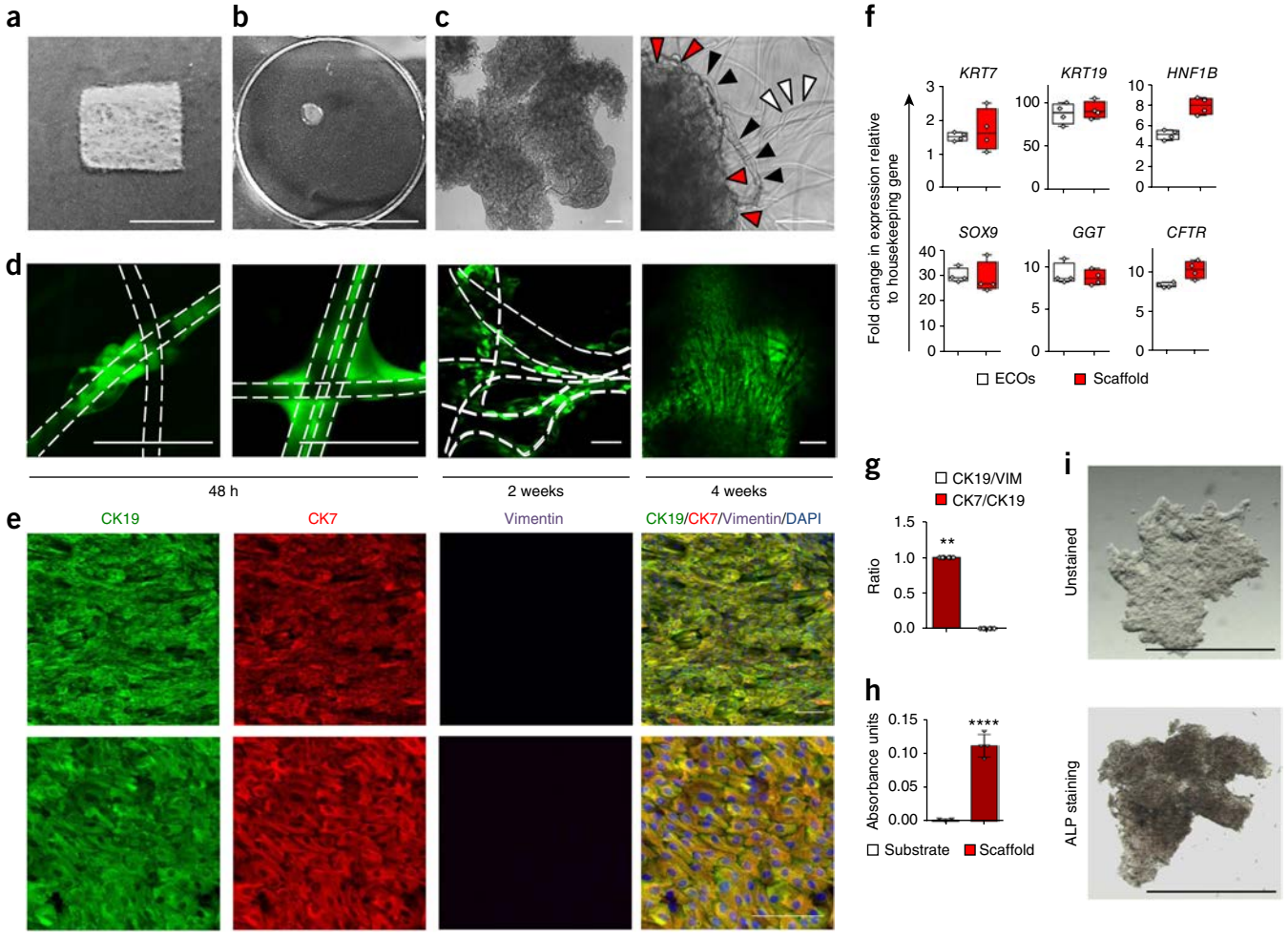

Figure 3 ECOs dissociated to single cells can populate biodegradable PGA scaffolds. (**a**,**b**) Photographs of a PGA scaffold before (**a**) and after (**b**) treatment with ECOs. Scale bars, 1 cm. Images are representative of three different scaffolds. (**c**) Light microscopy images of a PGA scaffold populated with ECOs dissociated to single cells. Red arrowheads, fully populated scaffold; black arrowheads, cells recruiting new PGA fibers; white arrowheads, PGA fibers. Scale bars, 100 µm. (**d**) Confocal microscopy images demonstrating cell expansion at different time points after seeding of single GFP$^+$ ECO cells on a PGA scaffold. White lines indicate the positions of the PGA fibers. Scale bars, 100 µm. (**e**) IF demonstrating expression of biliary markers and lack of expression of EMT markers by dissociated ECO cells seeded on PGA scaffolds. Scale bars, 100 µm. (**f**) qRT–PCR analyses demonstrating expression of biliary markers by ECOs before (ECOs) and after (scaffold) seeding on PGA scaffolds; $n = 4$ ECO lines. Center line, median; box, IQR; whiskers, range (minimum to maximum). Values are shown relative to those for the housekeeping gene *HMBS*. (**g**) Mean ratio of the numbers of CK7$^+$ and CK19$^+$ cells and CK19$^+$ and vimentin (VIM)$^+$ cells in IF analyses similar to the image shown in **e**. Error bars, s.d.; $n = 6$ cell lines; $^{**}P < 0.01$, Mann–Whitney test. (**h**) Mean GGT activity of dissociated ECO cells populating a PGA scaffold. Error bars, s.d.; $n = 4$ scaffolds; $^{****}P < 0.001$, two-tailed Student's *t*-test. (**i**) ALP staining of PGA scaffolds populated by dissociated ECO cells. Scale bars, 500 µm.

GFP-expressing ECOs into the injured animals (**Fig. 4a–g** and **Supplementary Fig. 10a–f**). Acellular PGA scaffolds and scaffolds populated with GFP-expressing fibroblasts (**Supplementary Fig. 11a–d**) were used as negative controls. Mice receiving acellular scaffolds died within 24 h of the operation (**Fig. 4b**), and post-mortem examination of these animals revealed yellow pigmentation of the peritoneal cavity and seminal vesicles, which is consistent with bile leak (**Supplementary Fig. 10a**); all animals in the group receiving fibroblast-populated scaffolds failed to reconstruct the gallbladder, which was replaced by fibrotic tissue incompatible with bile transport or storage (**Supplementary Fig. 11e–g**). In contrast, animals transplanted with ECO-populated scaffolds survived for up to 104 d without complications and were culled electively (**Fig. 4b**). Notably, the reconstructed gallbladders in the group transplanted with ECO-populated scaffolds were fully remodeled, with morphology resembling that of their native (untransplanted) counterparts (**Fig. 4c** and **Supplementary Fig. 10b**). Histology (**Fig. 4d**), IF and qRT–PCR analyses of the ECO-reconstructed gallbladders (**Fig. 4e** and **Supplementary Fig. 10c**,**d**) demonstrated integration of GFP$^+$ ECOs expressing biliary markers such as KRT19, KRT7, HNF-1β, SOX9, CFTR and a human-specific epitope for Ku80 (**Fig. 4e** and **Supplementary Fig. 10c**). Of note, the IF analyses also showed the presence of mouse mesenchymal cells expressing vimentin and endothelial cells expressing CD31 in the reconstructed biliary epithelium, suggesting that the scaffold is colonized by endogenous cells after transplantation (**Supplementary Fig. 10c**). Furthermore, we also identified a population of GFP$^+$vimentin$^+$CK19$^-$ cells, suggesting that ECOs may also contribute to the scaffold stroma *in vivo*, possibly through EMT (**Supplementary Fig. 10c**,**e**). The integrity of the reconstructed gallbladder lumen and its exposure to bile through continuity with the biliary tree were demonstrated using magnetic resonance cholangiopancreatography (MRCP) imaging before

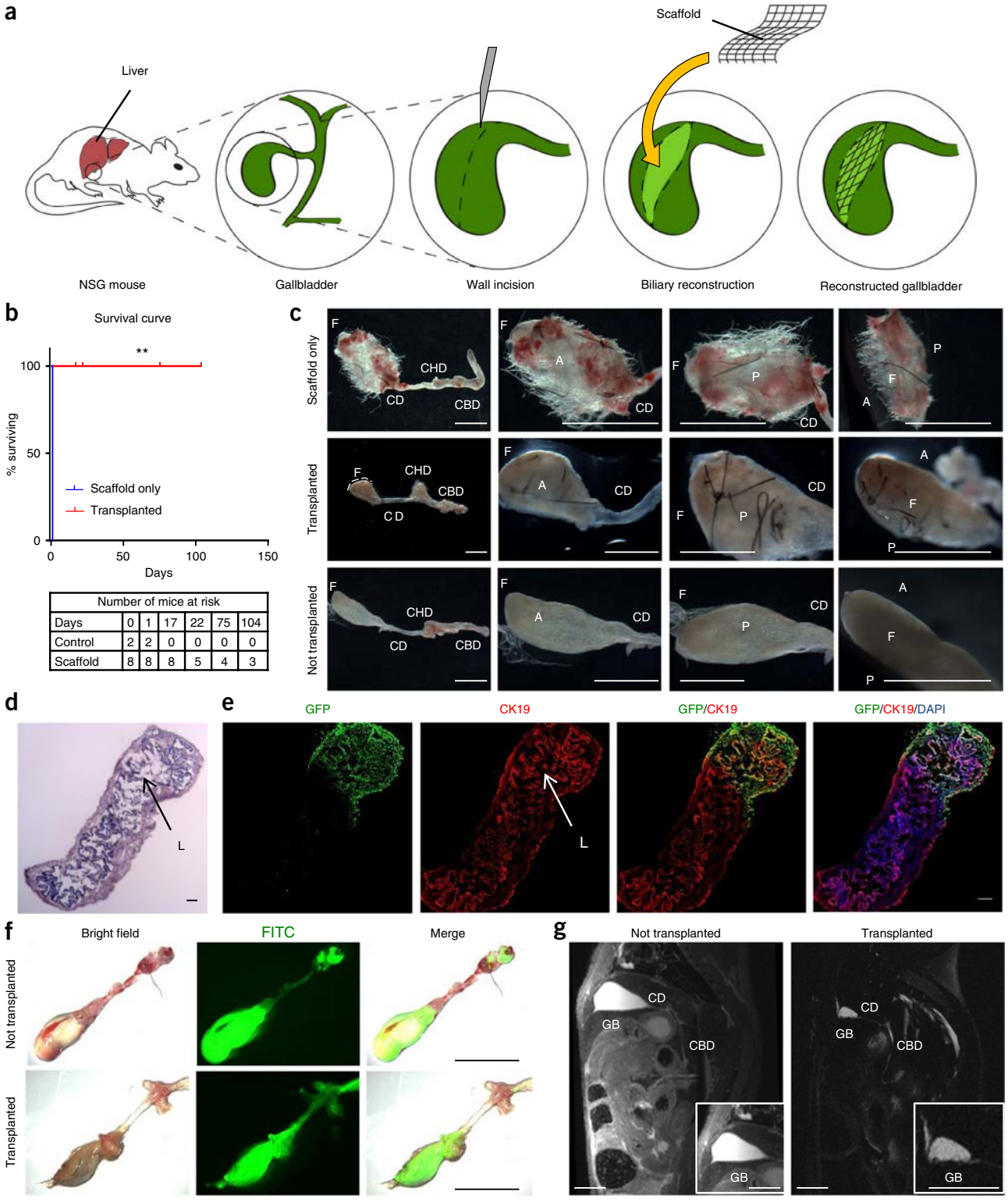

Figure 4 Biliary reconstruction in a mouse model of EHBI using ECOs. (**a**) Schematic representation of the method used for biliary reconstruction. (**b**) Kaplan–Meier survival analysis demonstrating rescue of mice with EHBI following biliary reconstruction with ECO-populated scaffolds. $^{**}P < 0.01$, log-rank test. (**c**) Images of gallbladders reconstructed with acellular PGA scaffold (scaffold only) or PGA scaffold populated with ECOs (transplanted) and native, non-reconstructed gallbladder control (not transplanted); gallbladders transplanted with ECO-populated scaffolds showed full reconstruction. CD, cystic duct; CBD, common bile duct; CHD, common hepatic duct; F, fundus; A, anterior surface; P, posterior surface. Scale bars, 500 μm. (**d**) H&E staining of a reconstructed gallbladder. L, lumen. Scale bar, 100 μm. (**e**) IF analyses demonstrating the presence of GFP^+ ECOs expressing biliary markers in reconstructed gallbladder. Scale bars, 100 μm. Higher-magnification images are provided in **Supplementary Figure 12**. (**f**,**g**) FITC cholangiogram ($n = 1$) (**f**) and MRCP images ($n = 2$) (**g**) of reconstructed (transplanted) versus native control (not transplanted) gallbladders (GB); the reconstructed gallbladders show a patent lumen and unobstructed communication with the rest of the biliary tree. Scale bars, 1 mm in **f** and 5 mm in **g**.

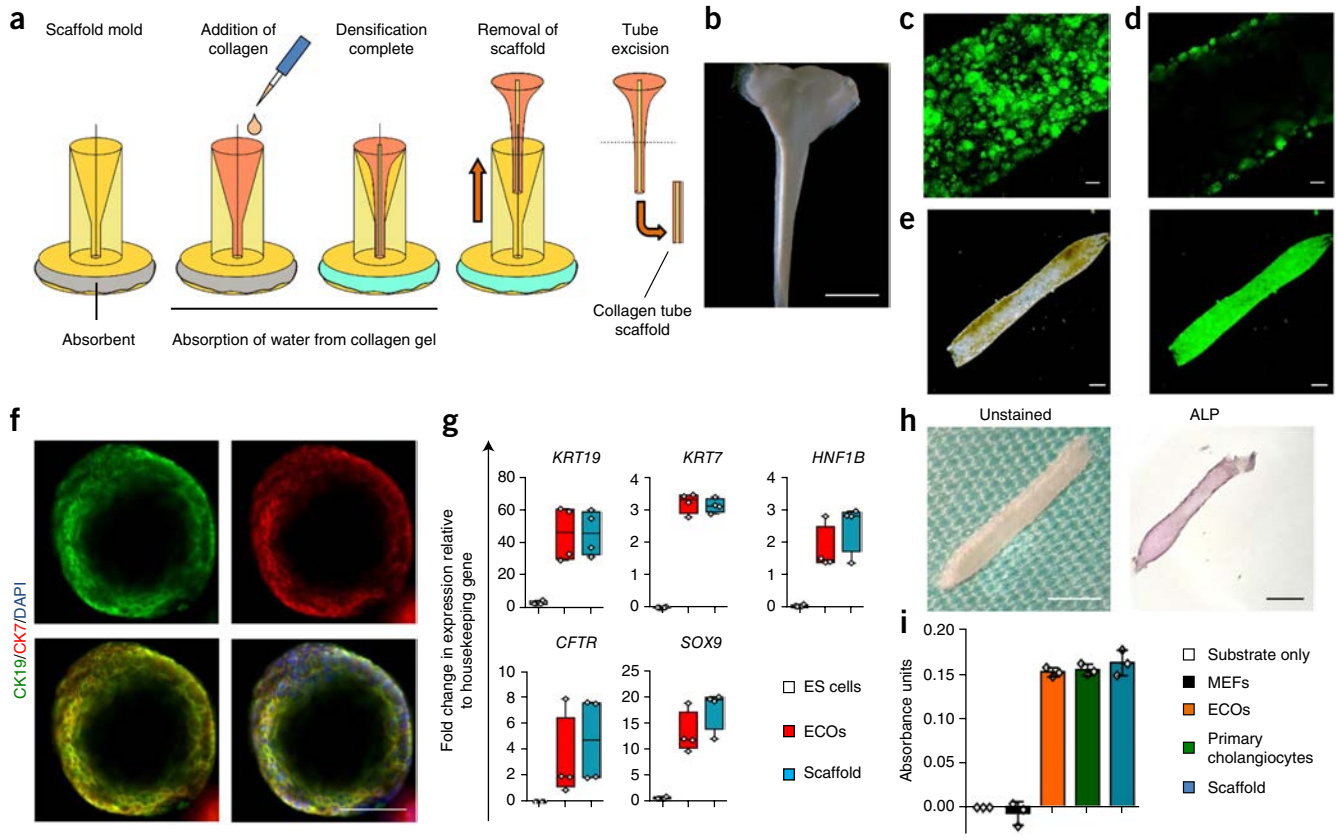

Figure 5 ECOs can populate tubular densified collagen scaffolds. (**a**) Schematic representation of the method used to generate tubular densified collagen scaffolds. (**b**) Image of a densified collagen construct before tube excision. Scale bar, 500 µm. (**c**) Maximum-intensity projection image depicting a tube populated with GFP$^+$ ECOs after its generation. Scale bar, 30 µm. (**d**) Confocal microscopy image showing the lumen patency of an ECO-populated collagen tube. Scale bar, 30 µm. (**e**) Bright-field (left) and fluorescence (right) images of a tube in which GFP$^+$ ECOs are nearly confluent. Scale bars, 100 µm. (**f**) IF analyses demonstrating the expression of biliary markers by ECOs following the generation of an ECO-populated tube. Scale bar, 100 µm. (**g**) qRT–PCR analyses demonstrating the expression of biliary markers by ECOs before (ECOs) and after (scaffold) the generation of ECO-populated collagen tubes. Embryonic stem cells were used as a negative control. $n = 4$ ECO lines; $n = 4$ ES lines. Center line, median; box, IQR; whiskers, range (minimum to maximum). Values are given relative to *HMBS* expression. (**h**,**i**) ECO-populated tubes exhibit ALP (**h**) and GGT (**i**) activity. Scale bars in **h**, 500 µm. MEFs, mouse feeder cells used as a negative control; scaffold, ECO-populated densified collagen tubes. Error bars in **g**, s.d.; $n = 3$ tubes.

removal of the organ and were further confirmed with fluorescein isothiocyanate (FITC) cholangiograms (**Fig. 4f**,**g**, **Supplementary Fig. 10f** and **Supplementary Video 1**). Post-mortem surgical examination and full-body magnetic resonance imaging performed 104 d following transplantation showed no evidence of tumor formation (**Supplementary Fig. 10f** and **Supplementary Video 2**), and IF analyses showed no GFP$^+$ cells in adjacent liver tissue (data not shown). In contrast, control gallbladders reconstituted with fibroblast exhibited obliteration of the gallbladder lumen (**Supplementary Fig. 11h**,**i**) and replacement of the lumen and biliary epithelium by fibroblasts expressing the fibroblast-specific antigen S100A4 (**Supplementary Fig. 11i**,**j**). When considered collectively, our findings demonstrate the capacity of ECOs to colonize their physiological niche and regenerate part of the biliary tree without any complications.

Bioengineered bile ducts replace the native mouse bile duct

Reconstruction of the gallbladder wall provided proof of principle for the capacity of ECOs to repair the biliary epithelium after injury; however, in the majority of extrahepatic bile duct disorders, the CBD is affected. Therefore, we focused on the generation of a tubular ECO-populated scaffold that could be used for bile duct replacement surgery. The internal diameter of the mouse CBD is approximately 100 µm and the wall thickness is <50 µm; these dimensions precluded the use of a PGA scaffold owing to mechanical properties. Instead, we generated tubular scaffolds of densified collagen (**Fig. 5a**,**b**) that were populated with GFP-expressing ECOs (**Fig. 5c**–**e**). The use of densified collagen enabled the generation of constructs with an external diameter ranging from 250–600 µm and adequate strength to maintain a patent lumen (**Fig. 5d**). Notably, the cells populating the collagen scaffolds maintained expression of biliary markers such as KRT19, KRT7, HNF-1β, SOX9 and CFTR (**Fig. 5f**,**g**) and exhibited GGT and ALP enzymatic activity (**Fig. 5h**,**i**). Primary epithelial cells of a different origin (human mammary epithelial cells, HMECs) failed to survive and adequately populate densified collagen tubes under the same conditions (**Supplementary Fig. 12a**). Moreover, plated HMECs failed to survive in a 10% bile solution (**Supplementary Fig. 12b**), further confirming the unique capacity of ECOs in generating bile-resistant bioengineered bile ducts. Collectively, these results demonstrate the capacity of ECOs to populate tubular densified collagen scaffolds without losing their original characteristics.

We then explored the possibility of replacing the native CBD of NGS mice with a bioengineered duct consisting of an ECO-populated

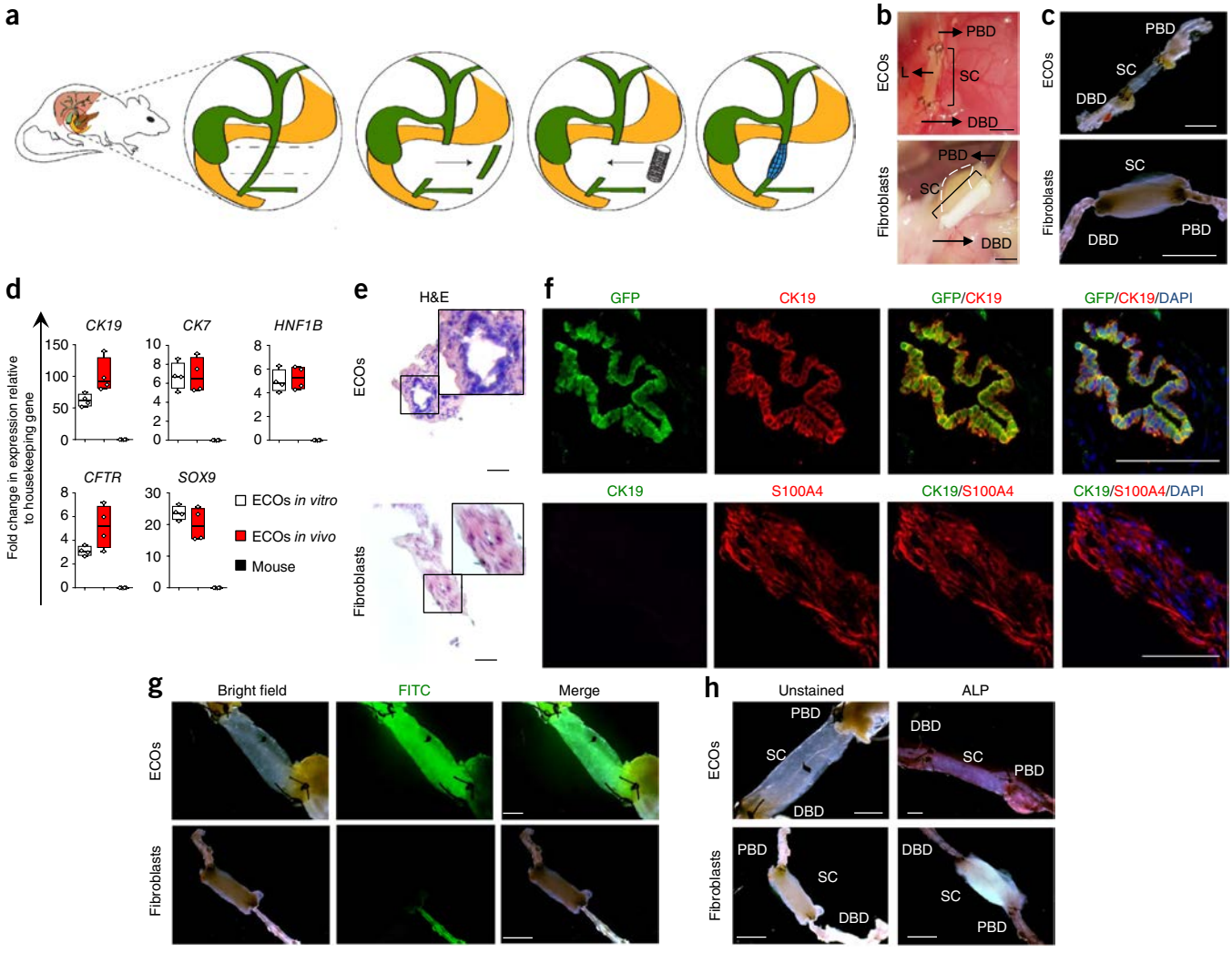

Figure 6 Bile duct replacement using ECO-populated densified collagen tubes. (**a**) Schematic representation of the method used for bile duct replacement. (**b**) Post-mortem images of mice that received an ECO-populated collagen tube (ECOs) versus a fibroblast-populated tube (fibroblasts). Bile flow results in yellow pigmentation of the ECO-populated tube. The white color of the fibroblast-populated conduit together with the dilated, bile-filled (yellow color) proximal bile duct (PBD) suggests luminal occlusion, resulting in bile leak (yellow peritoneal pigmentation, white dashed line). SC, collagen tubular scaffold; DBD, distal bile duct. Scale bars, 500 μm. (**c**) Images of a thin-walled construct resembling the native bile duct from a mouse receiving an ECO-populated tube versus a thickened construct with no distinguishable lumen from a mouse receiving a fibroblast-populated tube. Scale bars, 500 μm. (**d**) qRT–PCR analyses using human-specific primers confirming the expression of biliary markers by ECOs on the transplanted ECO-populated tubes (ECOs *in vivo*) as compared to cultured ECOs (ECOs *in vitro*) and mouse biliary tissue used as a negative control; $n = 4$ tubes. Center line, median; box, IQR; whiskers, range (minimum to maximum). Values are given relative to *HMBS* expression. (**e**) H&E staining demonstrating the presence of biliary epithelium and a patent lumen in an ECO-populated tube but not a fibroblast-populated construct. Scale bars, 100 μm. (**f**) IF analyses showing GFP^+CK19^+ epithelium lining the lumen of an ECO-populated construct versus obliteration of the lumen by fibroblasts in a fibroblast-populated construct. Scale bars, 100 μm. (**g**) FITC cholangiograms showing lumen patency in an ECO-populated tube versus occlusion of the lumen in a fibroblast-populated construct. Scale bars, 100 μm (ECOs) and 500 μm (fibroblasts). (**h**) ALP activity is observed only in ECO-populated tubes and not in fibroblast-populated constructs. Scale bars, 100 μm (ECOs) and 500 μm (fibroblasts).

densified collagen tube. A midportion of the native CBD was removed, and an ECO-populated collagen tube was anastomosed end to end to the proximal and distal duct remnants (**Fig. 6a**). Fibroblast-populated tubes were used as a negative control. Biliary reconstruction was achieved in all animals transplanted with ECO-populated tubes (**Fig. 6b**,**c** and **Supplementary Fig. 13a–d**), with mice followed up for up to 1 month post-transplantation (**Supplementary Fig. 13d**). Histology, IF and qRT–PCR analyses (**Fig. 6d–f** and **Supplementary Fig. 13a**,**b**) demonstrated a patent lumen, with the transplanted GFP^+ cells forming biliary epithelium (**Fig. 6e**,**f** and **Supplementary Fig. 13a**,**b**), and confirmed the expression of biliary markers such as KRT19, KRT7, HNF-1β, CFTR and SOX9 by the engrafted cells (**Fig. 6d**,**f** and **Supplementary Fig. 13b**). These analyses also illustrated the presence of mouse stromal and endothelial cells (**Supplementary Fig. 13b**). Moreover, we observed minimal apoptosis and proliferation in the transplanted tubes 1 month after transplantation, confirming the stability and integrity of the reconstituted biliary epithelium (**Supplementary Fig. 13b**,**c**). Lumen patency was further confirmed by FITC cholangiogram, MRCP and serum measurements of cholestasis markers (**Fig. 6g**, **Supplementary Fig. 13e**,**f** and **Supplementary Video 3**). Accordingly, animals receiving ECO-populated tubes exhibited no elevation in serum levels of

cholestasis markers (bilirubin and ALP; **Supplementary Fig. 13e**) and showed a patent lumen on imaging (**Fig. 6g** and **Supplementary Fig. 13f**), whereas bioartificial CBDs retained their ALP activity *in vivo* (**Fig. 6h**).

In contrast, all fibroblast-populated collagen tubes failed because of lumen occlusion (**Fig. 6b**,**c**,**e–g** and **Supplementary Fig. 13d**), resulting in high biliary pressures and bile leak through the site of anastomosis (**Fig. 6b**). In conclusion, our results demonstrate the capacity of ECO-populated collagen tubes to replace the native CBD *in vivo*.

DISCUSSION

We have demonstrated that epithelial cells from the extrahepatic biliary tree can be expanded and propagated *in vitro* while maintaining their cholangiocyte transcriptional signature and functional characteristics. In addition, our results show that primary cholangiocytes expanded *in vitro* as organoids have a unique potential in organ regeneration. Indeed, to our knowledge, our system provides the first proof of principle for the application of regenerative medicine in the context of CBD pathology. The capacity to replace a diseased CBD with an *in vitro*–bioengineered ECO-populated tube could have a considerable impact on the management of disorders such as biliary atresia, which constitutes the leading cause for pediatric liver transplantation[1], or ischemic strictures, which is one of the most common complications following transplantation[3]. Consequently, ECO-populated scaffolds represent a new system with high clinical relevance in the field of cholangiopathies.

Studies of the extrahepatic biliary epithelium have been limited by technical challenges in the long-term culture and large-scale expansion of primary cholangiocytes. These challenges have so far precluded large-scale experiments, such as transcriptomic and genome-wide analyses, which are urgently needed to better understand diseases of the bile duct such as PSC and cholangiocarcinoma. The capacity of ECOs for large-scale expansion could address this need. Indeed, we demonstrate that, starting from 10^5 extrahepatic cholangiocytes, we can generate from 10^{20}–10^{25} cells after 20 passages in culture. Therefore, ECOs not only represent a new source of cells for cell-based therapy but also provide a unique model system for studying the physiology and modeling disorders of the extrahepatic biliary tree *in vitro*.

Access to human tissue represents a considerable limitation for systems based on primary cells. However, we show that ECOs can be obtained not only from the CBD but also from the gallbladder. Gallbladder tissue is easily accessible and is routinely discarded following liver transplantation and cholecystectomy, one of the most common surgical procedures performed. Furthermore, in individuals not undergoing surgery, the CBD can be accessed using minimally invasive procedures such as ERCP, and we demonstrate that cholangiocytes can be obtained through brushings, which are routinely performed to acquire histology specimens. Notably, no morphological or functional differences were observed between organoids obtained with these different methods. Moreover, because of the scalability of our system, only a small amount of starting material is required. Finally, recent progress in replacing Matrigel with custom-made hydrogels to grow gut organoids[25] suggests that translating our system from Matrigel to a more clinically relevant good manufacturing practice (GMP)-compatible matrix could be feasible. When considered together, these approaches effectively address the challenges of tissue availability and create the possibility of cell-based therapy with autologous as well as allogeneic cells.

Notably, the derivation of primary hepatic stem cells using an organoid culture system has been reported previously[12]. However, the capacity of the resulting cells to differentiate into functional cholangiocytes and populate the biliary tree *in vivo* remains to be demonstrated. Furthermore, *in vivo* applications of such platforms could be restricted by contamination with stem cells that have a capacity to proliferate inappropriately after transplantation and/or differentiate into non-biliary cell types. Despite the association between organoids and adult stem cells[26], we never observed the expression of hepatocyte or pancreatic markers during our experiments, either *in vitro* or after transplantation, suggesting that the differentiation capacity of ECOs is limited to that of their lineage of origin. Moreover, canonical Wnt signaling, which is crucial for the expansion of adult stem cell organoids[27], is blocked in our culture conditions through the use of DKK-1; further studies may be required to fully elucidate the role of R-spondin in our system. Considered together, these observations suggest that our culture system does not include a stem cell population. However, we cannot completely exclude the possibility that these cells could represent a biliary progenitor cell population, on the basis of their ability to self-propagate and generate organoids from single cells (**Supplementary Video 4**).

Of note, we have recently established a system for the generation of cholangiocyte-like cells (CLCs) from human pluripotent stem cells[9]. However, it is worth noting that there are considerable differences between ECOs and CLCs. CLCs correspond to intrahepatic cholangiocytes, whereas ECOs represent the extrahepatic biliary epithelium. These two cell types are distinct in terms of embryological origin and disease involvement[14], and the two systems therefore complement each other for studies of the biliary tree. Indeed, CLCs are generated following a natural path of development and maintain fetal characteristics. Therefore, they provide a unique system for studies of human biliary development and developmental diseases, which are not possible using adult cells. However, CLCs may require a period of adjustment and further maturation *in vivo*, whereas mature, functional cells, such as ECOs, are required for coping with biliary injury in the acute setting and may be better suited for regenerative medicine applications. Furthermore, although human induced pluripotent stem cells represent a very good source of cells capable of generating almost any tissue, the initial derivation and characterization of these cell lines remains time-consuming and variability in differentiation capacity is still a challenge. ECOs can be derived in less than 24 h with very high efficiency and can be expanded through multiple passages without losing their original characteristics. Consequently, ECOs and CLCs are comparable in terms of scalability and are complementary in terms of applications, with the mature phenotype of ECOs providing a unique advantage for regenerative medicine applications in the context of tissue repair.

In conclusion, our results open up new avenues for the use of extrahepatic primary biliary tissue as a novel platform for *in vitro* studies, disease modeling and cell-based therapy applications.

METHODS

Methods, including statements of data availability and any associated accession codes and references, are available in the online version of the paper.

Note: Any Supplementary Information and Source Data files are available in the online version of the paper.

ACKNOWLEDGMENTS

The authors would like to thank J. Skepper, L. Carter and the University of Cambridge Advanced Imaging Centre for their help with electron microscopy; E. Farnell and the University of Cambridge, Cambridge Genomic Services for their help with microarray data processing and analysis; A. Petrunkina and the NIHR Cambridge BRC Cell Phenotyping Hub for their help with cell sorting; K. Burling and the MRC MDU Mouse Biochemistry Laboratory (MRC_MC_UU_12012/5)

for processing mouse serum samples; and R. El-Khairi for her help with IF images, R. Grandy for his help with providing relevant references, the Cambridge Biorepository for Translational Medicine for the provision of human tissue used in the study; D. Trono (Ecole Polytechnique Federale de Lausanne) for the gift of the plasmids used for the generation of GFP-expressing ECOs and B. McLeod for IT support. The monoclonal antibody TROMA-III, developed by R. Kemler, was obtained from the Developmental Studies Hybridoma Bank, created by the NICHD of the NIH and maintained at the University of Iowa.
This work was funded by ERC starting grant Relieve IMDs (281335; L.V., N.R.F.H.), the Cambridge Hospitals National Institute for Health Research Biomedical Research Centre (L.V., N.R.F.H., S. Sinha., F.S.), the Evelyn Trust (N.H.) and the EU FP7 grant TissuGEN (M.C.D.B.) and was supported in part by the Intramural Research Program of the NIH/NIAID (R.L.G., C.A.R.). F.S. has been supported by an Addenbrooke's Charitable Trust Clinical Research Training Fellowship and a joint MRC–Sparks Clinical Research Training Fellowship. (MR/L016761/1) A.W.J. and A.E.M. acknowledge support from EPSRC (EP/L504920/1) and an Engineering for Clinical Practice Grant from the Department of Engineering, University of Cambridge. J.B. was supported by a BHF Studentship (Grant FS/13/65/30441).

AUTHOR CONTRIBUTIONS

F.S. conceived and designed the study, performed experiments, acquired, interpreted and analyzed the data, developed and validated the protocols described, generated the figures, and wrote and edited the manuscript. A.W.J. generated the tubular densified collagen scaffolds and conceived and developed the manufacturing technique. O.C.T. contributed to cell culture and performed animal experiments, including kidney capsule injections and provision and dissection of mouse tissue. S. Sawiak performed the magnetic resonance imaging experiments. E.M.G. and S.S.U. reviewed and reported the magnetic resonance images. R.L.G. performed experiments, including animal experiments, IF and tissue histology. M.C.d.B. contributed to cell culture, generated viral particles, performed viral transduction experiments and generated GFP-expressing ECOs. N.L.B. and L. Valestrand performed animal experiments. M.J.G.-V. and P.M. performed bioinformatics analyses. D.O. performed flow cytometry analyses, and L.Y. performed immunoblot analyses. A.R. performed IF and qRT–PCR analyses and provided positive controls for IF and qRT–PCR. A.B. performed flow cytometry analyses and provided bioinformatics support. J.B. contributed to tissue histology and IF experiments. M.C.F.Z. contributed to PGA scaffold preparation and population with cells. M.T.P. generated viral particles, performed viral transduction experiments and generated GFP-expressing ECOs. M.P. generated viral particles. G.M.S. contributed to scaffold generation. P.M.M. and K.E.S. maintained and provided fibroblast controls. N.P. contributed to tissue culture. N.G. and C.A.R. contributed to dissection and provision of primary tissue. I.S. performed karyotyping and comparative genomic hybridization analyses. S.E.D. reviewed and reported the histology images. W.S., J.C., K.B.J., M.Z., S. Sinha, W.T.H.G., G.J.A., S.E.B., T.A.W., T.H.K. and E.M. contributed through critical revision of the manuscript for important intellectual content. N.R.F.H. contributed to the design and concept of the study and provided early study supervision. A.E.M. contributed to the design of the densified collagen scaffold and contributed through critical revision of the manuscript for important intellectual content. K.S.-P. provided primary tissue, performed animal experiments, including biliary reconstruction surgery, contributed to the design and concept of the study, supervised the study, interpreted the data, and wrote and edited the manuscript. L. Vallier designed and conceived the study, supervised the study, interpreted the data, and wrote and edited the manuscript. All of the authors approved the manuscript.

COMPETING FINANCIAL INTERESTS

The authors declare competing financial interests: details are available in the online version of the paper.

1. Murray, K.F. & Carithers, R.L. Jr. AASLD practice guidelines: evaluation of the patient for liver transplantation. *Hepatology* **41**, 1407–1432 (2005).
2. Perkins, J.D. Are we reporting the same thing? *Liver Transpl.* **13**, 465–466 (2007).
3. Skaro, A.I. *et al.* The impact of ischemic cholangiopathy in liver transplantation using donors after cardiac death: the untold story. *Surgery* **146**, 543–552, discussion 552–553 (2009).
4. Enestvedt, C.K. *et al.* Biliary complications adversely affect patient and graft survival after liver retransplantation. *Liver Transpl.* **19**, 965–972 (2013).
5. Gallo, A. & Esquivel, C.O. Current options for management of biliary atresia. *Pediatr. Transplant.* **17**, 95–98 (2013).
6. Felder, S.I. *et al.* Hepaticojejunostomy using short-limb Roux-en-Y reconstruction. *JAMA Surg.* **148**, 253–257, discussion 257–258 (2013).
7. Sampaziotis, F., Segeritz, C.-P. & Vallier, L. Potential of human induced pluripotent stem cells in studies of liver disease. *Hepatology* **62**, 303–311 (2015).
8. Kanno, N., LeSage, G., Glaser, S., Alvaro, D. & Alpini, G. Functional heterogeneity of the intrahepatic biliary epithelium. *Hepatology* **31**, 555–561 (2000).
9. Sampaziotis, F. *et al.* Cholangiocytes derived from human induced pluripotent stem cells for disease modeling and drug validation. *Nat. Biotechnol.* **33**, 845–852 (2015).
10. Sampaziotis, F. *et al.* Directed differentiation of human induced pluripotent stem cells into functional cholangiocyte-like cells. *Nat. Protoc.* **12**, 814–827 (2017).
11. LeSage, G., Glaser, S. & Alpini, G. Regulation of cholangiocyte proliferation. *Liver* **21**, 73–80 (2001).
12. Huch, M. *et al.* Long-term culture of genome-stable bipotent stem cells from adult human liver. *Cell* **160**, 299–312 (2015).
13. Masyuk, A.I., Masyuk, T.V. & LaRusso, N.F. Cholangiocyte primary cilia in liver health and disease. *Dev. Dyn.* **237**, 2007–2012 (2008).
14. Tabibian, J.H., Masyuk, A.I., Masyuk, T.V., O'Hara, S.P. & LaRusso, N.F. Physiology of cholangiocytes. *Compr. Physiol.* **3**, 541–565 (2013).
15. Cízková, D., Morký, J., Micuda, S., Osterreicher, J. & Martínková, J. Expression of MRP2 and MDR1 transporters and other hepatic markers in rat and human liver and in WRL 68 cell line. *Physiol. Res.* **54**, 419–428 (2005).
16. Gigliozzi, A. *et al.* Molecular identification and functional characterization of Mdr1a in rat cholangiocytes. *Gastroenterology* **119**, 1113–1122 (2000).
17. Xia, X., Francis, H., Glaser, S., Alpini, G. & LeSage, G. Bile acid interactions with cholangiocytes. *World J. Gastroenterol.* **12**, 3553–3563 (2006).
18. Caperna, T.J., Blomberg, A., Garrett, W.M. & Talbot, N.C. Culture of porcine hepatocytes or bile duct epithelial cells by inductive serum-free media. *In Vitro Cell. Dev. Biol. Anim.* **47**, 218–233 (2011).
19. Marinelli, R.A. *et al.* Secretin induces the apical insertion of aquaporin-1 water channels in rat cholangiocytes. *Am. J. Physiol.* **276**, G280–G286 (1999).
20. Gong, A.-Y. *et al.* Somatostatin stimulates ductal bile absorption and inhibits ductal bile secretion in mice via SSTR2 on cholangiocytes. *Am. J. Physiol. Cell Physiol.* **284**, C1205–C1214 (2003).
21. Ito, M. *et al.* NOD/SCID/γ_c^{null} mouse: an excellent recipient mouse model for engraftment of human cells. *Blood* **100**, 3175–3182 (2002).
22. Chan, B.P. & Leong, K.W. Scaffolding in tissue engineering: general approaches and tissue-specific considerations. *Eur. Spine J.* **17** (Suppl. 4), 467–479 (2008).
23. Cheung, H.-Y., Lau, K.-T., Lu, T.-P. & Hui, D. A critical review on polymer-based bio-engineered materials for scaffold development. *Compos., Part B Eng.* **38**, 291–300 (2007).
24. Jabłonska, B. End-to-end ductal anastomosis in biliary reconstruction: indications and limitations. *Can. J. Surg.* **57**, 271–277 (2014).
25. Gjorevski, N. *et al.* Designer matrices for intestinal stem cell and organoid culture. *Nature* **539**, 560–564 (2016).
26. Koo, B.K. & Clevers, H. Stem cells marked by the R-spondin receptor LGR5. *Gastroenterology* **147**, 289–302 (2014).
27. Farin, H.F., Van Es, J.H. & Clevers, H. Redundant sources of Wnt regulate intestinal stem cells and promote formation of Paneth cells. *Gastroenterology* **143**, 1518–1529. e7 (2012).

[1]Wellcome Trust–Medical Research Council Stem Cell Institute, Cambridge Stem Cell Institute, Anne McLaren Laboratory, University of Cambridge, Cambridge, UK. [2]Department of Surgery, University of Cambridge and NIHR Cambridge Biomedical Research Centre, Cambridge, UK. [3]Department of Hepatology, Cambridge University Hospitals NHS Foundation Trust, Cambridge, UK. [4]Department of Engineering, University of Cambridge, Cambridge, UK. [5]Department of Clinical Neurosciences, University of Cambridge, Cambridge, UK. [6]Department of Radiology, Cambridge University Hospitals NHS Foundation Trust, Cambridge, UK. [7]Immunopathogenesis Section, Laboratory of Parasitic Diseases, National Institute of Allergy and Infectious Diseases, US National Institutes of Health, Bethesda, Maryland, USA. [8]Norwegian PSC Research Center, Department of Transplantation Medicine, Division of Surgery, Inflammatory Diseases and Transplantation, Oslo University Hospital, Rikshospitalet, Oslo, Norway. [9]Cambridge Genomic Services, Department of Pathology, University of Cambridge, Cambridge, UK. [10]Department of Medicine, School of Clinical Medicine, University of Cambridge, Cambridge, UK. [11]Division of Cardiovascular Medicine, University of Cambridge, Cambridge, UK. [12]University Department of Paediatrics, University of Cambridge, Cambridge, UK. [13]Department of Paediatric Gastroenterology, Hepatology and Nutrition, Cambridge University Hospitals NHS Foundation Trust, Cambridge, UK. [14]Division of Cardiovascular Medicine, University of Cambridge, Cambridge, UK. [15]Biotech Research and Innovation Centre (BRIC), University of Copenhagen, Copenhagen, Denmark. [16]Wellcome Trust Sanger Institute, Hinxton, UK. [17]School of Engineering and Physical Sciences, Heriot-Watt University, Edinburgh, UK. [18]Department of Biomedical Engineering, University of Strathclyde, Glasgow, UK. [19]Department of Surgery, University of Edinburgh, Edinburgh Royal Infirmary, Edinburgh, UK. [20]NIHR Cambridge Biomedical Centre (BRC) hIPSCs Core Facility, Addenbrooke's Hospital, University of Cambridge, Cambridge, UK. [21]University of North Carolina, Chapel Hill, School of Medicine, Chapel Hill, North Carolina, USA. [22]Medical Genetics Laboratories, Cambridge University Hospitals NHS Trust, Cambridge, UK. [23]Department of Histopathology, Cambridge University Hospitals NHS Foundation Trust, Cambridge, UK. [24]Center for Biomolecular Sciences, University of Nottingham, Nottingham, UK. [25]Nottingham Digestive Diseases Centre, NIHR Nottingham Biomedical Research Centre at the Nottingham University Hospitals NHS Trust and University of Nottingham, Nottingham, UK. [26]These authors contributed equally to this work. [27]These authors jointly directed this work. Correspondence should be addressed to L. Vallier (lv225@cam.ac.uk).

ONLINE METHODS

Primary biliary tissue. Primary biliary tissue (bile duct or gallbladder) was obtained from deceased organ donors from whom organs were being retrieved for transplantation. The gallbladder or a section of the bile duct was excised during the organ retrieval operation after obtaining informed consent from the donor's family (REC reference numbers: 12/EE/0253, NRES Committee East of England, Cambridge Central and 15/EE/0152 NRES Committee East of England, Cambridge South).

Isolation of primary cholangiocytes. Excised bile duct segments were placed in a 10-cm plate and washed once with William's E medium (Gibco, Life Technologies). A longitudinal incision was made along the wall of the excised bile duct segment, exposing the lumen, and 10–15 ml of William's E medium was added to cover the tissue. The luminal epithelium was subsequently scraped off using a surgical blade while the tissue was submerged in medium. The supernatant was collected, and the tissue and plate were washed two or three times with William's E medium to collect any remaining cells. The supernatant and washes were combined and centrifuged at 444*g* for 4 min. The pellet was washed with William's E medium and recentrifuged; the supernatant was discarded (**Fig. 1a**).

Excised gallbladders were placed in a 15-cm plate, a longitudinal incision was made along the wall of the excised gallbladder and the lumen was washed once with William's E medium (Gibco, Life Technologies). Cholangiocytes were isolated following the method described above (**Supplementary Fig. 2a**).

For cholangiocyte isolation through brushing, an excised bile duct segment was placed in a 10-cm plate and cannulated using an ERCP brush. The luminal surface was brushed 10–20 times, and the cells were collected by washing the brush several times in a Falcon tube containing 40–50 ml of William's E medium (**Supplementary Fig. 2b**).

Generation and culture of ECOs. Isolated primary cholangiocytes were centrifuged at 444*g* for 4 min and resuspended in a mixture of 66% Matrigel (BD Biosciences, 356237) and 33% William's E medium (Gibco, Life Technologies) supplemented with 10 mM nicotinamide (Sigma-Aldrich), 17 mM sodium bicarbonate (Sigma-Aldrich), 0.2 mM 2-phospho-L-ascorbic acid trisodium salt (Sigma-Aldrich), 6.3 mM sodium pyruvate (Invitrogen), 14 mM glucose (Sigma-Aldrich), 20 mM HEPES (Invitrogen), ITS + premix (BD Biosciences), 0.1 μM dexamethasone (R&D Systems), 2 mM Glutamax (Invitrogen), 100 U/ml penicillin and 100 μg/ml streptomycin, 20 ng/ml EGF (R&D Systems), 500 ng/ml R-spondin (R&D Systems) and 100 ng/ml DKK-1 (R&D Systems). The cell suspension was plated in a 24-well plate format at 50 μl/well so that a small dome of Matrigel formed in the center of each well, and plates were then incubated at 37 °C for 10–30 min until the Matrigel solidified. Subsequently, 1 ml of William's E medium with supplements was added to each well. The culture medium was changed every 48 h.

To split the cells, Matrigel was digested by adding Cell Recovery Solution (Corning) for 30 min at 4 °C. The resulting cell suspension was collected, centrifuged at 444*g* for 4 min, washed once with William's E medium and resuspended in 66% Matrigel and 33% William's E medium with supplements, as described above.

All experiments were performed using passage 20 ECOs unless otherwise stated.

Cell line identity. Demographic data for the donor corresponding to each ECO line are provided in **Supplementary Table 1**. Following derivation, ECO lines were authenticated by matching their karyotype (**Supplementary Fig. 4b**) to the sex of the donor. The lines were tested on a regular basis and found to be negative for mycoplasma contamination.

Immunofluorescence, RNA extraction and qRT–PCR. IF analysis, RNA extraction and qRT–PCR were performed as previously described[9]. A complete list of the primary and secondary antibodies used is provided in **Supplementary Table 3**. A complete list of the primers used is provided in **Supplementary Table 4**.

All qRT–PCR data are presented as the median, interquartile range (IQR) and range (minimum to maximum) of four independent ECO lines unless otherwise stated. Values are given relative to that of the housekeeping gene hydroxymethylbilane synthase (*HMBS*).

All IF images were acquired using a Zeiss Axiovert 200M inverted microscope or a Zeiss LSM 700 confocal microscope. ImageJ 1.48k software (Wayne Rasband, NIH; http://imagej.nih.gov/ij) was used for image processing. IF images are representative of three different experiments. IF images of reconstructed gallbladder sections are representative of five different animals.

Microarrays. RNA was assessed for concentration and quality using a SpectroStar (BMG Labtech) and a Bioanalyzer (Agilent Technologies). Microarray experiments were performed at Cambridge Genomic Services, University of Cambridge, UK, using the HumanHT-12 v4 Expression BeadChip (Illumina) according to the manufacturer's instructions. Briefly, 200 ng of total RNA underwent linear amplification using the Illumina TotalPrep RNA Amplification Kit (Life Technologies) following the manufacturer's instructions. The concentration, purity and integrity of the resulting cDNA were measured by SpectroStar and Bioanalyzer. Finally, cDNA was hybridized to the HumanHT-12 v4 BeadChip overnight, and the arrays were subsequently washed, stained and scanned using the Bead Array Reader (Illumina). The RNA used for microarray analysis was collected from three different ECO lines ($n = 3$). Microarray experiments were performed at Cambridge Genomic Services, University of Cambridge, UK, using the HumanHT-12 v4 Expression BeadChip (Illumina) according to the manufacturer's instructions.

Microarray analysis. Raw data were loaded into R using the lumi package from Bioconductor[28] and divided into subsets according to the groups being compared; only the samples involved in a given comparison were used. Subsets were then filtered to remove any nonexpressed probes using the detection *P* value from Illumina. Across all samples, probes for which the intensity value was not statistically significantly different ($P > 0.01$) from those of the negative controls were removed from the analysis. Following filtering, the data were transformed using Variance Stabilization Transformation[29] from lumi and then normalized to remove technical variation between arrays using quantile normalization. Comparisons were performed using the limma package[30], with results corrected for multiple testing using false discovery rate (FDR) correction. Finally, the quality of the data was assessed, along with the correlations between samples within groups.

Probes differentially expressed between hepatocytes and ECOs representing the aggregate transcriptional 'signature' of ECOs were selected for Euclidean hierarchical clustering using Perseus software (MaxQuant). Standard scores (*z*-scores) were calculated for the $\log_2$-normalized probe expression values across the different conditions and used for this analysis. Heat maps and principal-component analysis (PCA) plots were generated using MaxQuant Perseus software (http://www.perseus-framework.org/)[31]. Functional annotation and GO analyses were performed on genes that were differentially expressed between primary cholangiocytes and ECOs (**Fig. 1d**) using the NIAID/NIH Database for Annotation, Visualization and Integrated Discovery (DAVID) v6.8 (https://david.ncifcrf.gov/)[32,33].

Western blot analysis. Total protein was extracted with lysis buffer (50 mM Tris pH 8, 150 mM NaCl, 0.1% SDS, 0.5% sodium deoxycholate, 1% Triton X-100, and protease and phosphatase inhibitors). Protein concentrations were determined using the BCA Protein Assay Kit (Thermo Fisher Scientific) according to the manufacturer's instructions. Samples were prepared for western blot analysis by adding 1× NuPAGE LDS Sample Buffer with 1% β-mercaptoethanol and were incubated for 5 min at 95 °C. Protein (25 μg) was separated by 4–12% NuPAGE Bis-Tris protein gel (Invitrogen) and transferred onto polyvinylidene difluoride (PVDF) membrane (Bio-Rad). Proteins were detected by probing with antibodies specific to phospho-β-catenin (Ser33/Ser37/Thr41) (Cell Signaling Technology, 9561), active β-catenin (Millipore, 05-665), total β-catenin (R&D, AF1329) and β-tubulin (Sigma, T4026), which was followed by incubation with horseradish-peroxidase-conjugated anti-mouse, anti-goat or anti-rabbit secondary antibodies. Membranes were developed using Pierce ECL western blotting substrate (Thermo Scientific) according to the manufacturer's instructions. The raw western blot images are provided in **Supplementary Figure 14**. Validation information for each of these antibodies is available on the relevant manufacturer's website.

doi:10.1038/nm.4360

Rho kinase activity analyses. Rho kinase activity was measured using a commercially available kit (Cell Biolabs, STA-416) according to the manufacturer's instructions.

Flow cytometry analyses. ECOs were collected using Cell Recovery Solution (Corning) for 30 min at 4 °C and were then centrifuged at 444*g* for 4 min and dissociated to single cells using TrypLE Express (Gibco). Cells were subsequently fixed using 4% paraformaldehyde (PFA) for 20 min at 4 °C. Cell staining and flow cytometry analyses were performed as previously described[9,34].

Karyotyping. ECOs were collected using Cell Recovery Solution (Corning), dissociated to single cells as described above, plated in gelatin-coated plates and cultured using William's E medium with supplements. When cells were subconfluent, usually after 72 h, the cultures were incubated for 3–4 h with William's E medium with supplements containing 0.1 μg/ml colcemid (Karyomax, Gibco). Cells were then collected using trypsin-EDTA (0.05%) (Gibco) for 4–5 min at 37 °C, centrifuged at 344*g* for 5 min and resuspended in 5 ml of KCl hypotonic solution (0.055 M). The suspension was recentrifuged at 344*g* for 5 min, 2 ml of a 3:1 100% methanol:glacial acetic acid solution was added and slides were prepared as previously described[35].

Comparative genomic hybridization analyses. Genomic DNA was labeled using the BioPrime DNA Labeling Kit (Invitrogen) according to the manufacturer's instructions, and samples were hybridized to Agilent Sureprint G3 unrestricted CGH ISCA 8×60K human genome arrays following the manufacturer's protocol, as previously described[36]. The data were analyzed using Agilent CytoGenomics Software.

Rhodamine 123 transport assay. Rhodamine 123 transport assays were performed as previously described[9], and images were acquired using a Zeiss LSM 700 confocal microscope. Fluorescence intensity was measured between the organoid interior and exterior, and luminal fluorescence was normalized to the background level for the extraluminal space. Each experiment was performed in triplicate. Error bars represent s.d.

Cholyl-lysyl-fluorescein transport assay. To achieve loading with CLF (Corning), ECOs were split in 5 μM CLF and incubated at 37 °C for 30 min. Images were acquired using a Zeiss LSM 700 confocal microscope, and fluorescence intensity was measured between the organoid interior and exterior as described for the rhodamine 123 transport assay. To demonstrate that the observed changes in CLF fluorescence intensity were secondary to active export of CLF from the organoid lumen, the experiment was repeated with 5 μM unconjugated FITC (Sigma-Aldrich) as a control. Fluorescence intensity measurement was performed as described for the rhodamine 123 transport assay. Each experiment was performed in triplicate. Error bars represent s.d.

γ-glutamyl transferase activity. GGT activity was measured in triplicate using the MaxDiscovery GGT Enzymatic Assay Kit (Bioo Scientific) based on the manufacturer's instructions. Error bars represent s.d. Absorbance units refer to light absorbance at a wavelength of 405 nm.

Alkaline phosphatase staining. ALP staining was carried out using the BCIP/NBT color development substrate (5-bromo-4-chloro-3-indolyl-phosphate/nitro blue tetrazolium) (Promega) according to the manufacturer's instructions.

Responses to secretin and somatostatin. Responses to secretin and somatostatin were assessed as previously described[9].

Generation of ECOs expressing GFP. EGFP-expressing VSV-G pseudotyped recombinant HIV-1 lentiviral particles were produced with an optimized second-generation packaging system by transient cotransfection of three plasmids into HEK-293T cells (ATCC, CRL-11268). EGFP expression is under the control of a core EF-1α promoter. All plasmids were a gift from D. Trono and obtained from Addgene (pWPT-GFP, 12255; psPAX2, 12260; pMD2.G, 12259). Viral infection of organoids was performed as previously described[37]. Infected ECOs were expanded for two passages, collected as described above for flow cytometry analyses and cell sorted by flow cytometry for GFP^+ cells. GFP-expressing single cells were plated using our standard plating method and cultured in William's E medium with supplements for 1–2 weeks until fully grown ECOs developed.

Generation of ECO-populated PGA scaffolds. One-millimeter-thick PGA scaffolds with a PGA density of 50 mg/cm^3 were used for all experiments. Prior to cell seeding, the PGA scaffolds were pretreated with 1 M NaOH for 10–30 s, washed three times, decontaminated in a 70% ethanol solution for 30 min and then air-dried for another 30 min until all of the ethanol had fully evaporated. All scaffolds were a gift from S. Sinha and obtained from Biomedical Structures (Biofelt).

ECOs were collected and dissociated into single cells as previously described for flow cytometry analyses; 5–10 × 10^6 cells were resuspended in 100 μl of William's E medium with supplements and seeded on a scaffold surface area of 1 cm^2. Scaffolds were incubated at 37 °C for 30–60 min to allow the cells to attach. The scaffolds were placed in the wells of a 24-well plate and checked at regular intervals during this period to ensure that the medium did not evaporate. If necessary, 10–20 μl of William's E medium with supplements was added. After 1 h, 2–3 ml of William's E medium with supplements was added to the wells, and the medium was subsequently changed twice weekly.

Generation of densified collagen tubes. Densified collagen tubes were prepared using a novel approach. A 3D printed chamber was fabricated, consisting of a funnel piece and a base plate. A 250-μm-thick metallic wire was mounted into the base plate and fed through the center of the funnel. Absorbent paper towels were compacted between the two 3D printed parts, which were then screwed together. Collagen gel solution (5 mg/ml), loaded with cells, was poured into the funnel and gelled at 37 °C for 30 min. The screws were then loosened, and water was drawn out of the collagen gel by placing the 3D printed chambers at 37 °C for 2–4 h. A cell-loaded densified collagen tube was thus formed with a 250-μm lumen and a wall thickness of 30–100 μm, determined by the duration of the drying phase. Upon removal from the chamber, the tube was trimmed for excess collagen and cut to the required length.

Culture of HMECs. HMECs and the required tissue culture consumables were purchased as a kit from Lonza (CC-2551B), and the cells were cultured according to the supplier's instructions. The cells were tested for mycoplasma by the manufacturer.

Animal experiments. All animal experiments were performed in accordance with UK Home Office regulations (UK Home Office Project License numbers PPL 80/2638 and PPL 70/8702). Immunodeficient NSG mice, which lack B, T and NK lymphocytes[38], were bred in house, and food and water were available *ad libitum* before and after procedures. A mix of male and female animals aged approximately 6–8 weeks was used. All of the ECO constructs used were populated with ECOs derived from human CBD.

Generation of the extrahepatic biliary injury mouse model. To generate a model of EHBI, midline laparotomy was performed and the gallbladder was mobilized by dividing the ligamentous attachment connecting its fundus to the anterior abdominal wall under isoflurane general anesthesia. A longitudinal incision was then made along two-thirds of the length of the gallbladder, from the fundus toward Hartmann's pouch (the neck of the gallbladder).

Biliary reconstruction in EHBI mice. To reconstruct the gallbladder, a scaffold section measuring approximately 1 × 1 mm^2 (seeded with ECOs or lacking ECOs in controls) was sutured as a 'patch' to close the defect using 4–6 interrupted 10-0 nonabsorbable nylon sutures under 40× magnification. The laparotomy was closed in two layers with continuous 5-0 absorbable Vicryl sutures. The animals were given buprenorphine (temgesic; 0.1 mg/kg) analgesia as a bolus and observed every 15 min in individual cages until fully recovered.

Eight animals underwent biliary reconstruction using an ECO-populated scaffold. All these animals survived to 104 d after surgery without complications and were culled electively for further analyses. Two control experiments were performed where the animals underwent biliary reconstruction using acellular

scaffolds. Both animals died within 24 h from bile leak; therefore, no further control experiments were performed to minimize animal discomfort.

Bile duct replacement. The native CBD was divided, and a short segment was excised. The populated densified collagen tube was anastomosed end to end, using interrupted 10-0 nylon sutures, between the divided proximal and distal CBD segments. A length of 5-0 nylon suture material (diameter, 100 μm) was inserted into the collagen tube and fed into the proximal and distal CBD segments to ensure patency of the lumen during anastomosis. After anastomosis was complete, the 5-0 suture was pushed into the duodenum through the distal bile duct and was removed through an incision in the duodenum, which was then closed with interrupted 10-0 nylon sutures. Lumen patency was assessed at the time of transplantation through light microscopy and cannulation of the lumen with a 5-0 nonabsorbable suture. Transplantation was abandoned as futile in the case of fully occluded tubes due to cell infiltration. These events were considered to represent construct failure rather than surgical complications and were therefore not censored in the survival analysis.

Bile duct ligation. C57BL/6 mice were purchased from The Jackson Laboratory. Mice were housed and bred in a Minimal Disease Unit at the animal facility at Oslo University Hospital, Rikshospitalet, Oslo, Norway. All experiments were performed on male mice aged 8–12 weeks. Median laparotomy was performed, and the CBD was exposed and ligated close to the junction of the hepatic bile ducts. Sham-operated mice underwent the same procedure without ligation. Serum was collected after 5 d. Alanine transaminase (ALT), aspartate transaminase (AST) and ALP levels were measured in serum using an ADVIA 1800 instrument (Siemens) at the Central Laboratory, Norwegian School of Veterinary Science. All animal experiments were approved by the Norwegian Food Safety Authority (project license no. FOTS 8210/15), and all animals received humane care in line with the NIH Guide for the Care and Use of Laboratory Animals.

Blood sample collection. Blood was taken using a 23-gauge needle directly from the inferior vena cava under terminal anesthesia at the time the animals were electively culled and transferred into 1.5-ml Eppendorf tubes for further processing.

Blood sample processing. Blood samples were routinely processed by the University of Cambridge Core Biochemical Assay Laboratory (CBAL). All sample analysis was performed on a Siemens Dimension EXL analyzer using reagents and assay protocols supplied by Siemens.

Light microscopy imaging. Light microscopy images of excised reconstructed gallbladders were acquired using a Leica MZFLIII fluorescence dissecting microscope. The images are representative of five animals.

Cryosectioning and histology. Excised gallbladders were fixed in 4% PFA, immersed in sucrose solution overnight, mounted in optimal cutting temperature (OCT) compound and stored at −80 °C until sectioning. Sections were cut to a thickness of 10 μm using a cryostat microtome and mounted on microscopy slides for further analysis.

H&E staining. H&E staining was performed using Sigma-Aldrich reagents according to the manufacturer's instructions. Briefly, tissue sections were hydrated, treated with Meyer's hematoxylin solution for 5 min (Sigma-Aldrich), washed with warm tap water for 15 min, placed in distilled water for 30–60 s and incubated with eosin solution (Sigma-Aldrich) for 30–60 s. Sections were subsequently dehydrated and mounted using Eukitt quick-hardening mounting medium (Sigma-Aldrich). Histology sections were reviewed by an independent histopathologist with a special interest in hepatobiliary histology (S.D.).

TUNEL assay. TUNEL assays were performed using a commercially available kit (Abcam, ab66110) according to the manufacturer's instructions.

FITC cholangiography. *In situ* FITC cholangiography was performed in euthanized animals after dissection of the gallbladder from adherent liver lobes but before surgical interruption of the extrahepatic biliary tree. The distal bile duct was cannulated with a 23½-gauge needle, FITC was injected in retrograde into the gallbladder and images were taken under a fluorescent microscope.

Magnetic resonance cholangiopancreatography. MRCP was performed after euthanization of the animals and was carried out at 4.7 T using a Bruker BioSpec 47/40 system. A sequence with rapid acquisition followed by relaxation enhancement was used with an echo train length of 40 echoes at 9.5-ms intervals, a repetition time of 1,000 ms and a field of view of $5.84 \times 4.18 \times 4.18$ cm^3 with a matrix of $256 \times 180 \times 180$ pixels, yielding an isotropic resolution of 230 μm. The actively decoupled four-channel mouse cardiac array provided by Bruker was used for imaging.

For the second mouse imaged, a 2D sequence was used with slightly varied parameters (24 echoes spaced at 11-ms intervals to give an effective echo time of 110 ms, repetition time of 5,741 ms, matrix size of 256×256, field of view of 4.33×5.35 cm^2; yielding a planar resolution of 170×200 μm^2) for a higher signal-to-noise ratio to improve visualization of the biliary ducts. Fifteen 0.6-mm slices were acquired coronally through the liver and gallbladder. For acquisition, a volume coil was used to reduce the impact of radiofrequency inhomogeneity.

The biliary duct and gallbladder images were prepared by maximum-intensity projection. Structural imaging to rule out neoplastic growth was performed using a T1-weighted 3D FLASH (fast low-angle shot) sequence with a flip angle of 25°, a repetition time of 14 ms and an echo time of 7 ms. The matrix was $512 \times 256 \times 256$ with a field of view of $5.12 \times 2.56 \times 2.56$ cm^3, for a final isotropic resolution of 100 μm.

The MRCP images were reviewed by two independent radiologists with a special interest in hepatobiliary radiology (E.M.G. and S.U.).

Statistical analyses. All statistical analyses were performed using GraphPad Prism 6. For small sample sizes, where descriptive statistics were not appropriate, individual data points were plotted. For comparison of two mean values, a two-sided Student's *t*-test was used to calculate statistical significance. Normal distribution of our values was confirmed using the D'Agostino–Pearson omnibus normality test where appropriate. Variance between samples was tested using the Brown–Forsythe test. To compare multiple groups to a reference group, one-way ANOVA with Dunnett's correction for multiple comparisons was used for groups with equal variance and the Kruskal–Wallis test with Dunn's correction for multiple comparisons was applied for groups with unequal variance. Survival was compared using log-rank (Mantel–Cox) tests. Where given, the number of replicates (n) refers to the number of ECO lines or the number of different animals, unless otherwise stated. Further details of the statistical analyses performed are provided in **Supplementary Table 5**.

For animal experiments, group sizes were estimated on the basis of previous study variance. Final animal group sizes were chosen to allow elective culling at different time points while maintaining $n > 4$ animals surviving past 30 d to ensure reproducibility. No statistical methods were used to calculate sample size. No formal randomization method was used to assign animals to study groups. However, littermate animals from a given cage were randomly assigned to experimental or control groups by a technician not involved in the study. No animals were excluded from the analysis. No blinding was used when only one group of animals survived for radiology imaging. In cases where more than one group survived to be imaged, such as when gallbladders were reconstructed with fibroblasts versus ECOs, both radiologists reviewing the images (E.G. and S.U.) where blinded to the method of reconstruction.

Data availability. The microarray data are open access and available online on ArrayExpress under accession code E-MTAB-4591.

28. Du, P., Kibbe, W.A. & Lin, S.M. lumi: a pipeline for processing Illumina microarray. *Bioinformatics* **24**, 1547–1548 (2008).
29. Lin, S.M., Du, P., Huber, W. & Kibbe, W.A. Model-based variance-stabilizing transformation for Illumina microarray data. *Nucleic Acids Res.* **36**, e11 (2008).
30. Smyth, G.K. Linear models and empirical Bayes methods for assessing differential expression in microarray experiments. *Stat. Appl. Genet. Mol. Biol.* **3**, Article3 (2004).

doi:10.1038/nm.4360

31. Tyanova, S. *et al.* The Perseus computational platform for comprehensive analysis of (prote)omics data. *Nat. Methods* **13**, 731–740 (2016).
32. Huang, W., Sherman, B.T. & Lempicki, R.A. Systematic and integrative analysis of large gene lists using DAVID bioinformatics resources. *Nat. Protoc.* **4**, 44–57 (2009).
33. Huang, W., Sherman, B.T. & Lempicki, R.A. Bioinformatics enrichment tools: paths toward the comprehensive functional analysis of large gene lists. *Nucleic Acids Res.* **37**, 1–13 (2009).
34. Bertero, A. *et al.* Activin/nodal signaling and NANOG orchestrate human embryonic stem cell fate decisions by controlling the H3K4me3 chromatin mark. *Genes Dev.* **29**, 702–717 (2015).
35. Campos, P.B., Sartore, R.C., Abdalla, S.N. & Rehen, S.K. Chromosomal spread preparation of human embryonic stem cells for karyotyping. *J. Vis. Exp.* http://dx.doi.org/10.3791/1512 (2009).
36. Hannan, N.R.F. *et al.* Generation of multipotent foregut stem cells from human pluripotent stem cells. *Stem Cell Reports* **1**, 293–306 (2013).
37. Koo, B.-K., Sasselli, V. & Clevers, H. Retroviral gene expression control in primary organoid cultures. *Curr. Protoc. Stem Cell Biol.* **27**, Unit 5A.6 (2013).
38. Shultz, L.D. *et al.* Human lymphoid and myeloid cell development in NOD/LtSz-scid IL2Rγ^{null} mice engrafted with mobilized human hemopoietic stem cells. *J. Immunol.* **174**, 6477–6489 (2005).